Electrical Power and Energy Systems 162 (2024) 110327

Contents lists available at ScienceDirect

International Journal of Electrical Power and Energy Systems

journal homepage: www.elsevier.com/locate/ijepes

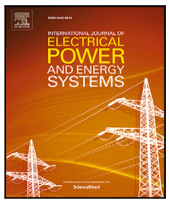

Data-driven continuous-time framework for frequency-constrained unit commitment

Mohammad Rajabdorri [a,*], Enrique Lobato [a], Lukas Sigrist [a], Jamshid Aghaei [b]

[a] Instituto de Investigación Tecnológica (IIT), Escuela Técnica Superior de Ingeniería (ICAI), Universidad Pontificia Comillas, Madrid, Spain
[b] School of Engineering and Technology, Central Queensland University, Queensland, Australia

ARTICLE INFO

Keywords:
Frequency-constrained unit commitment
Continuous-time formulation
Data-driven frequency nadir
Start-up and shut-down trajectories
Bernstein polynomials

ABSTRACT

The conventional approach to solving the unit commitment problem involves discrete intervals at an hourly scale, particularly when integrating frequency dynamics to formulate a frequency-constrained unit commitment. To overcome this limitation, a novel continuous-time frequency-constrained unit commitment framework is proposed in this paper. In this approach, Bernstein polynomials represent continuous variables in the unit commitment problem and enable the calculation of frequency response-related metrics such as the rate of change of frequency, quasi-steady-state frequency, and frequency nadir, and the corresponding continuous-time constraints are introduced. Notably, startup and shut-down trajectories are meticulously considered, transforming the formulation into a fully continuous-time model and simplifying constraints related to variable continuity. To address the complexities associated with integrating the obtained non-linear frequency nadir constraint into a mixed-integer linear problem, an alternative data-driven frequency nadir constraint is proposed, which accurately constrains frequency nadir deviations throughout the time interval. To validate the proposed model, it is applied to the real-life network of the Spanish Island of La Palma. The data-driven method for estimating frequency nadir has demonstrated a minimum accuracy of 99.61% and has consistently maintained the frequency above the defined threshold.

1. Introduction

Thanks to the recent progress, the short-term load and RES forecasts are more accurate than ever [1–4]. Although forecasting methods are improving rapidly, the forecasted quantities should be discretized into energy blocks (usually 1-h) when used for operation planning. The use of discrete forecasted load and RES forecasts in unit commitment (UC) yields discrete generation and reserve schedules. The use of such discrete intervals is a source of error by neglecting sub-hourly changes in demand and RES for instance. As it is not physically feasible to instantaneously ramp up/down at hourly intervals, independent system operators (ISOs) would employ different ways to make that possible. For example, California ISO instructs a 20-min linear ramp across the hourly intervals [5]. The deviation of the forecasted quantities from the actual quantities will be treated in subsequent planning and real-time operation steps, leading to additional costs. These variations can be significant in island power systems, where RES generation is geographically located in a few areas, for instance, and can cause variations in the sub-hourly generation dispatch with respect to the expected one.

Low-inertia power systems in general and island power systems in particular are sensitive to active power disturbances, causing significant frequency variations. The importance of inertia in power grids, especially with the increase in RES and DC transmission, is highlighted in [6]. The most challenging disturbances are generation outages in islands. UC formulations considering post-disturbance frequency dynamics have been proposed in the literature [7–14]. Ensuring the adequacy of frequency response is more crucial than ever, as the system inertia is declining because of the growing implementation of non-synchronous RES. If the frequency response is not sufficient when a grid-related event happens, load shedding happens, and if not done rapidly, cascading events leading to a blackout will occur. This emphasizes the importance of identifying and maintaining frequency deviations [15].

In [7] a stochastic UC method optimizes various frequency services concurrently, specifically tailored for low inertia systems featuring substantial RES integration. Employing scenario trees generated through a quantile-based scenario generation approach, the stochastic model addresses the challenge of linearizing frequency nadir. The technique involves an inner approximation method for one side of the equation

* Corresponding author.
E-mail address: mrajabdorri@comillas.edu (M. Rajabdorri).

https://doi.org/10.1016/j.ijepes.2024.110327
Received 6 May 2024; Received in revised form 9 July 2024; Accepted 20 October 2024
Available online 31 October 2024

Acronyms

CFCUC	Continuous-time frequency constrained unit commitment
CUC	Continuous-time unit commitment
FCUC	Frequency constrained unit commitment
HVDC	High-voltage direct current
ISO	Independent system operator
MILP	Mixed integer linear programming
RES	Renewable energy sources
RoCoF	Rate of change of frequency
SD	Shut-down
SU	Start-up
UC	Unit commitment

Nomenclature

Bernstein Polynomials

$\beta_{b,n}(\tau)$	Bernstein basis function
τ	Time variable
b	Index of the Bernstein coefficient [$\in \{0,\dots,n-1\}$]
$f(\tau)$	A function of τ
n	Degree of Bernstein polynomial
${B'_n}^f(\tau)$	Differential of Bernstein polynomial
${B_n}^f(\tau)$	Bernstein polynomial of order n for function f
${C_b}^f$	bth Bernstein coefficient to represent f

CUC

$\mathcal{I}$	Set of all generators
$\overline{D}$	Demand [MW]
$\overline{\mathcal{P}}_i$	Maximum power output of generator i [MW]
$\overline{\mathcal{R}}_i$	Maximum ramp-up of generator i [MW/h]
DT	Minimum down-time of generators [h]
gc(.)	Generation costs [k€]
suc(.)	Start-up costs [k€]
UT	Minimum up-time of generators [h]
$\underline{\mathcal{P}}_i$	Minimum power output of generator i [MW]
$\underline{\mathcal{R}}_i$	Maximum ramp-down of generator i [MW/h]
i	Index of generators
p'	Differential of power [MW/s]
p	Power generation variable [MW]
p^{RES}	RES generation variable [MW]
r	Online reserve power variable [MW]
s	Alias index for time intervals
T	Set of all time intervals
t	Index of time intervals
u_i	Commitment variable [$\in \{0,1\}$]
v_i	Start-up variable [$\in \{0,1\}$]
w_i	Shut-down variable [$\in \{0,1\}$]

MILP CUC

$\boldsymbol{\beta}$	Vector of Bernstein basis functions
$\boldsymbol{D}$	Vector of load coefficients
$\boldsymbol{P}$	Vector of power coefficients
$\boldsymbol{P}^{\text{RES}}$	Vector of RES coefficients
$\boldsymbol{P}^{\text{curt}}$	Vector of curtailment coefficients
SD_i^T	Shut-down time duration of unit i [h]
SU_i^T	Start-up time duration of unit i [h]
$C_{b,t,i}$	bth Benstein coefficient at time t of unit i

CFCUC

α	Coefficients in the linear model
$\boldsymbol{R}$	Vector of reserve coefficients
$\Delta f^{\text{ss}}_{\text{crit}}$	Critical steady-state frequency [Hz]
$\Delta f'_{\text{crit}}$	Critical RoCoF [Hz/s]
ℓ	Index of the lost unit
D	Load damping factor [%/Hz]
f^{nadir}	Frequency nadir [Hz]
f_0	Nominal frequency [Hz]
H_ℓ	Available weighted inertia after outage of ℓ [MW s]
T^g	Delivery time of the units [s]

and utilizes binary expansion, linearized through the big-M technique, for the other side. in [8] a linear formulation is presented, addressing the UC problem by incorporating details about inertial response and system frequency response. This formulation ensures adequate ancillary service provision to prevent under-frequency load shedding after the biggest outage. To linearize the frequency nadir constraint, they calculate first-order partial derivatives of its equation for higher-order non-linear variables, ultimately representing the frequency nadir through a set of piecewise linearized constraints. In [9] the differential–algebraic equation of the frequency response is piecewise approximated using Bernstein polynomials and then linearized, to reflect frequency nadir. The frequency constrained unit commitment (FCUC) that is proposed in [16] integrates an emergency frequency control strategy utilizing the transient overload capabilities of high-voltage direct current (HVDC) systems for inertial response. Additionally, it introduces an AC–DC primary response model considering HVDC decline rates, facilitating optimized AC–DC secondary response solutions. A method for obtaining frequency constraints in low-inertia grids, focusing on the optimal allocation of distributed energy storage systems for locational frequency security, is proposed in [17]. In [18] a dynamic frequency response model is analyzed to derive the relation between frequency nadir and reserve power. In the day-ahead scheduling stage, optimal power reserve for distributed generators is determined to satisfy the primary and secondary frequency regulation.

In contrast to deriving analytical formulas from the swing equation employed in [7,8,10,16] adopts a data-driven multivariate optimal classification trees technique. They propose a robust formulation to address load and RES uncertainties. The classification tree is independently solved as a mixed integer linear programming (MILP) problem. A dynamic model for generating training data is contributed in [11], which is utilized subsequently in training a deep neural network. The trained neural networks are structured for integration into an MILP problem, facilitating the development of a frequency nadir predictor for application in the UC problem. In [12] a conservative sparse neural network is used to learn the frequency dynamics. Then the learned model is encoded as MILP to be incorporated into the UC problem. A robust formulation with data-driven frequency constraint is proposed in [13], and in [14] frequency nadir constraint is obtained, using a synthetically generated dataset.

An unwritten assumption in these studies is that power is delivered in hourly constant blocks and the outage of the unit during an hour yields the same frequency response. In reality, outages can happen

at any moment throughout the time interval, and power outputs are subjected to intra-hour changes. When an outage happens depending on the instantaneous power output of the units, the frequency response might be different. To be able to restrain the frequency response continuously throughout the time interval, we should formulate the UC problem as a continuous-time model. In [19] a continuous-time model based on Bernstein polynomials is introduced. As the output of CUC presented in [19] is a continuous curve, it also captures the ramping of the units. So this CUC can ensure there are enough ramping resources to handle the evergrowing variabilities in the power system and larger ramping events. The adequacy of ramping resources should be ensured, particularly due to the addition of solar power, which exacerbates the need for fast ramping units in the early morning and early evening hours [20]. Bernstein polynomials are further utilized in [21] to develop a novel continuous-time optimization model for co-optimizing balancing energy and flexible ramp products in real-time power system's operation. These polynomials are employed to model the continuous trajectories of up and down flexible ramp products, ensuring the deliverability of ramping capacity. And in [22] by employing Bernstein polynomials, the function-space optimization is converted into MILP for tractable calculation. While employing Bernstein polynomials instead of the traditional discrete UC formulation may introduce additional computational burden and potentially impact scalability, it is not a concern in this context. This paper's emphasis is on low-inertia island power systems, which tend to be relatively small in scale.

The CUC formulation of [19] is employed as a starting point for the proposed CFCUC. Frequency response metrics like rate of change of frequency, quasi-steady-state frequency, and frequency nadir are obtained from the swing equation and defined as Bernstein polynomials in this paper. In the case of frequency nadir, the obtained term is highly non-linear, which makes it hard to calculate and apply to the MILP problem in hand, even after considering the simplifying assumptions that are suggested later in the methodology section. To avoid that, a data-driven approach is utilized to acquire a linear frequency nadir constraint similar to [14]. Linear regression is employed to drive the frequency nadir constraint from this synthetic dataset in terms of Bernstein coefficients. Data-driven methods are proven to be effective in describing frequency dynamics in the FCUC problem [10–14]. It is revealed in the results section that the simplifying assumption and the learning procedure can continuously restrict the frequency nadir deviation very accurately throughout the time interval.

Another useful addition to the proposed CFCUC formulation is start-up (SU) and shut-down (SD) trajectories, which are ignored in [19]. Power trajectories during SU and SD are mostly neglected in the UC formulation. However, units are providing energy and ramp during the SU and SD process. Optimally scheduling these trajectories is economically and technically favorable and is studied in [23–26]. It is claimed in [23] that the traditional UC may result in false estimations of the ramping capability of the units. Then, it presents a linear continuous schedule of generation that better fits the load profile and considers SU and SD trajectories. In [27] the authors analyze the potential of short-time SU and SD regulation modes of thermal units to regulate system peak load. An optimal scheduling model is proposed, which includes an improved UC model incorporating SU and SD trajectories of thermal units.

We particularly consider SU and SD trajectories because (1) the CFCUC model will be fully continuous. (2) The zero-order continuity (which ensures the continuity of the scheduled power outputs) and the first-order continuity (which ensures the continuity of the derivative of the power outputs, i.e. the continuity of ramping) of Bernstein polynomials between intervals will be preserved, even when the start-up or shut-down of the units. (3) As claimed in [24] the model will be tighter and faster, which is very useful to alleviate the computational burden of the proposed CFCUC. The cited studies are summarized in Fig. 1. References with discrete formulation are shown dashed and the ones that use Bernstein polynomials with continuous lines. The ones that consider SU and SD trajectories with a solid bullet, and the ones that consider frequency constraints with =.

The contributions with respect to the previous studies as follows.

- The frequency-related metrics are defined as continuous-in-time Bernstein polynomials, and the respective constraints are applied to the CUC problem.
- The obtained frequency nadir equation based on Bernstein polynomials is highly non-linear. A data-driven approach is suggested to drive a linear frequency nadir constraint. The dataset is generated with a synthetic procedure, introduced in [14]. Simplifying assumptions are offered, to calculate the frequency nadir and label the sample data points.
- SU and SD trajectories are included in the CUC formulation to improve its solution run-time and general representation.

The rest of the paper is organized as follows. The methodology is presented in Section 2 which includes an introduction to the required basic of Bernstein polynomial (in Section 2.1), a general formulation of CUC (in Section 2.2), and the proposed FCUC (in Section 2.4). The obtained results are demonstrated in Section 3. Finally, the conclusions are drawn in Section 4.

2. Methodology

As mentioned before, the continuous variables in CUC are defined as Bernstein polynomials. In this section, first, the necessary fundamentals about the Bernstein polynomials to define the CUC are described. Then it is used to build the general CUC and the proposed CFCUC models.

2.1. Bernstein polynomials

2.1.1. Function approximation

Bernstein's function can approximate curves with a linear combination of polynomials. One advantage of using polynomials is that they can be calculated very quickly algebraically. For a function $f(\tau)$, defined on the closed interval ($\tau \in [0,1]$), the expression ${B_n}^f(\tau)$ is called the Bernstein polynomial of order n for the function $f(\tau)$,

$$ {B_n}^f(\tau) = \sum_{b=0}^{n} {C_b}^f \times \beta_{b,n}(\tau), \tag{1} $$

where ${C_b}^f$ is the Bernstein coefficient and for $f(\tau)$ is equal to $f\left({}^{b}/_{n}\right)$. ${B_n}^f(\tau)$ is a polynomial in τ of order n and $\beta_{b,n}(\tau)$ are the Bernstein basis functions.

$$ \beta_{b,n}(\tau) = \binom{n}{b} \tau^b (1-\tau)^{n-b} \tag{2} $$

If $f(\tau)$ is continuous on $[0,1]$, it is proven that the following equation is true in $[0,1]$,

$$ \lim_{n\to\infty} {B_n}^f(\tau) = f(\tau) \tag{3} $$

So if the order on n is sufficiently high ${B_n}^f(\tau) \approx f(\tau)$. In this paper, Bernstein polynomials of order 3 are used to describe continuous variables in each interval. Fig. 2 shows all Bernstein basis functions of order 3. This figure may help visualize how Bernstein polynomial functions approximate curves. It is straightforward to extend the definition of a Bernstein polynomial in $[0,1]$ to $[t, t+1]$.

2.1.2. Useful propositions

Here, some of the useful propositions of the Bernstein polynomials that will help us to develop our proposed method are introduced.

Proposition 2.1. *Differentiating (1) with respect to τ leads to:*

$$ {B'_n}^f(\tau) = n \sum_{b=0}^{n-1} \left({C_{b+1}}^f - {C_b}^f\right) \binom{n-1}{b} \tau^b (1-\tau)^{n-1-b} \tag{4} $$

Eq. (4) is a Bernstein polynomial of order $n-1$. Here, ${C_{b+1}}^f - {C_b}^f$ is the difference of the first order $\Delta f({}^{b}/_{n})$ of the function $f(\tau)$ at $\tau = {}^{b}/_{n}$ [28].

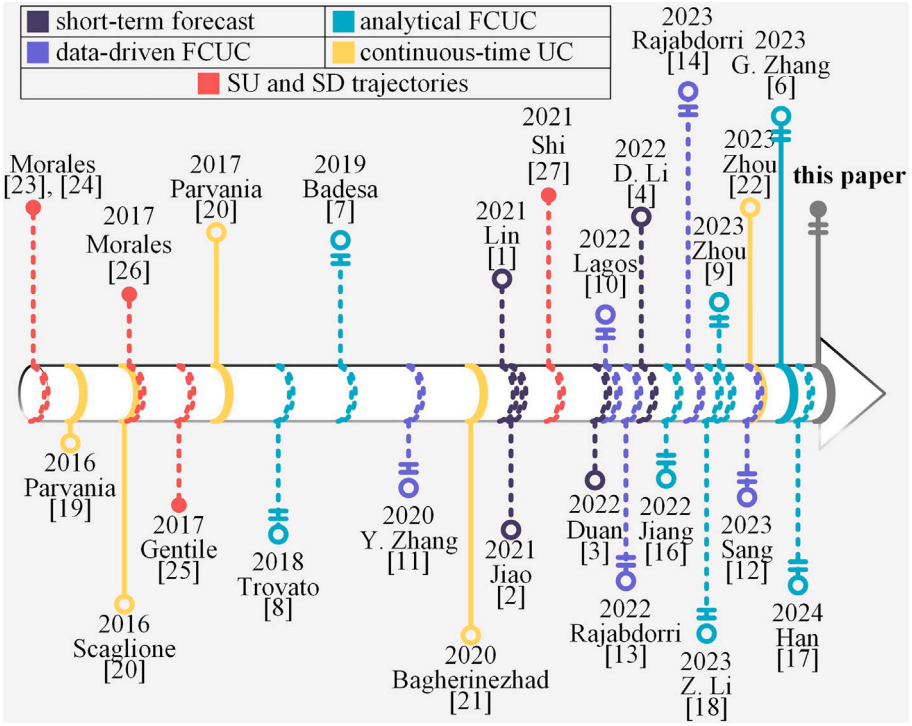

Fig. 1. Summary of the cited studies.

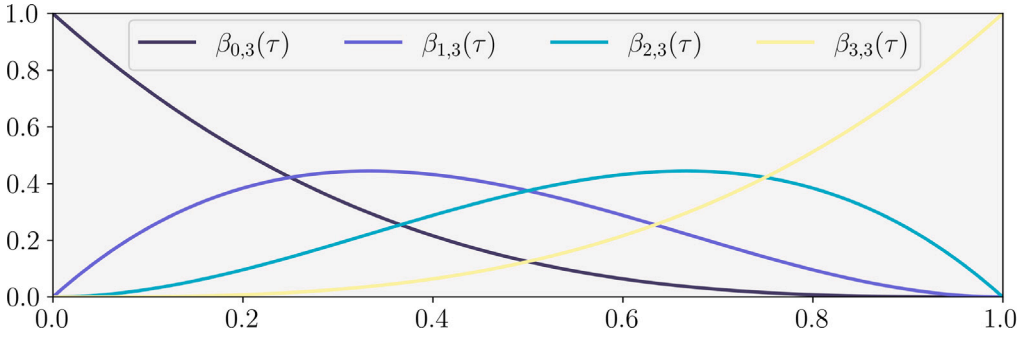

Fig. 2. Bernstein basis functions of order 3.

Proposition 2.2. *Convex hull property indicates that ${B_n}^f(\tau)$ will never be outside the convex hull of the control polygon formed by Bernstein coefficients for each b. That is, ${B_n}^f(\tau)$ is always between maximum and minimum coefficients.*

$$\max_{\forall b}\left({C_b}^f\right) \le {B_n}^f(\tau) \le \min_{\forall b}\left({C_b}^f\right) \tag{5}$$

A general property of Bernstein polynomials, as concluded from [29], is that it satisfies the convex hull property. Each Bernstein polynomial of order n consists of n different terms, each of them is the production of a coefficient ${C_b}^f$ and a Bernstein basis function. This property significantly helps, later when maximum and minimum generations and ramping constraints are derived. Because of this property and other features mentioned in [30], Bernstein polynomials are convenient to use for solving CFCUC problem, and especially to define and implement the frequency nadir constraint in the proposed CFCUC.

Proposition 2.3. *The sum and difference of two polynomials of the same degree can be effortlessly calculated by adding or subtracting their respective Bernstein coefficients [31].*

And if the order of polynomials does not match, the one with the lower order should be elevated until they have the same order. Elevating ${B_n}^f(\tau)$ means finding a Bernstein polynomial with higher order m ($m > n$) such that ${B_m}^f(\tau) = {B_n}^f(\tau)$.

Proposition 2.4. *The new bth Bernstein coefficients after elevating ${B_n}^f(\tau)$ by one are calculated as,*

$$\frac{b}{n+1}{C_{b-1}}^f + (1-\frac{b}{n+1}){C_b}^f \tag{6}$$

Proposition 2.4 can be done recursively to increase the order.

Proposition 2.5. *to multiply two Bernstein Polynomials of ${B_n}^f(\tau)$ and ${B_m}^g(\tau)$ that are defined on the same interval, the product will be of order $n+m$ and the kth coefficients of the product are given by*

$${C_k}^{fg} = \sum_{j=\max(0,k-m)}^{\min(n,k)} \frac{\binom{n}{j}\binom{m}{k-j}}{\binom{n+m}{k}} {C_j}^f {C_{k-j}}^g \tag{7}$$

where $k \in \{0, \dots, n+m\}$.

2.2. CUC formulation

Solving the UC problem determines the schedule of all generating units in the system by considering their constraints and supplying

the forecasted load at minimum cost. A general CUC formulation is expressed below [19],

$$\min_{u,p} \ \mathrm{suc}\big(u(\tau)\big) + \mathrm{gc}\big(p_i(\tau)\big) \tag{8a}$$

$$u_i(\tau) - u_i(\tau-1) = v_i(\tau) - w_i(\tau) \qquad \tau \in T,\ i \in \mathcal{I} \tag{8b}$$

$$v_i(\tau) + w_i(\tau) \le 1 \qquad \tau \in T,\ i \in \mathcal{I} \tag{8c}$$

$$\int_{\tau-\mathrm{UT}_i+1}^{\tau} v_i(\tau)d\tau \le u_i(\tau) \qquad \tau - \mathrm{UT}_i + 1 \ge 0,\ i \in \mathcal{I} \tag{8d}$$

$$\int_{\tau-\mathrm{DT}_i+1}^{\tau} w_i(\tau)d\tau \le 1 - u_i(\tau) \qquad \tau - \mathrm{DT}_i + 1 \ge 0,\ i \in \mathcal{I} \tag{8e}$$

$$p_i(\tau) \ge \underline{P}_i u_i(\tau) \qquad \tau \in T,\ i \in \mathcal{I} \tag{8f}$$

$$p_i(\tau) + r_i(\tau) \le \overline{P}_i u_i(\tau) \qquad \tau \in T,\ i \in \mathcal{I} \tag{8g}$$

$$p_i'(\tau) \ge \underline{\mathcal{R}}_i \qquad \tau \in T,\ i \in \mathcal{I} \tag{8h}$$

$$p_i'(\tau) \le \overline{\mathcal{R}}_i \qquad \tau \in T,\ i \in \mathcal{I} \tag{8i}$$

$$\sum_{i\in\mathcal{I}} \big(p_i(\tau)\big) + p^{\mathrm{RES}}(\tau) = \mathcal{D}(\tau) \qquad \tau \in T \tag{8j}$$

The objective is to minimize Eq. (8a), where suc(·) is the start-up cost and gc(·) is the generation cost function. Eq. (8a) is subjected to Eqs. (8b) to (8j). Eqs. (8b) and (8c) represent the binary logic of the UC problem. Eqs. (8d) and (8e) are the continuous representation of the units' minimum up-time and minimum downtime constraints. Eqs. (8f) and (8g) are the minimum and the maximum power generation constraints respectively. Eqs. (8h) and (8i) are ramp-down and ramp-up constraints. Eq. (8j) is the power balance equation. This formulation leads to a complex and computationally intractable time-variant problem, that is, it is not straightforward to solve.

2.3. MILP formulation of CUC

The following approximations and modifications are provided to convert this intractable problem into a MILP. Doing so enables us to use MILP techniques that are fairly fast and already developed. The Bernstein approximation is used to fit the load curve and forecasted wind generation. In this method, all continuous curves are divided into one-hour intervals ($[t, t+1]$) and each interval is approximated by a Bernstein polynomial of order three. Higher-order polynomials can be used if more accuracy is needed. The output will be the optimized continuous-time generation of units, also represented by Bernstein polynomials of order 3. Thus the optimization variables are the Bernstein coefficients of the power output of the units. Ramping schedule of units is defined as the differentiation of generation. According to Eq. (4), if the generation is of order 3, ramping will be presented by Bernstein polynomials of order 2. It is assumed that the binary variables can only change value at the beginning of an hour, so they are not defined as Bernstein polynomials. That follows the traditional way of committing the units.

Different parts of Eqs. (8a) to (8j) are reformulated as follows to achieve a formulation that is representable as MILP. In this formulation, the SU and SD power trajectories are also considered. The simplifying assumptions in this paper regarding the SU and SD trajectories are: (1) the duration of the SU process and the SD process is assumed to be SU_i^T and SD_i^T, respectively and (2) the unit is at its minimum output power at the end (beginning) of the SU (SD) process. Note that the other assumption in [23–26] regarding a linear variation of the power in time during SU and SD process is not needed here, as the Bernstein polynomials will describe the ramping.

2.3.1. Load approximation

Each hourly interval $[t, t+1]$ of the input load is approximated by a Bernstein polynomial of order 3. This approximation is more accurate than the hourly discrete approximation used in practice (see Fig. 3, where the Bernstein polynomial almost perfectly follows the 5-min forecast). Each interval is defined as the product of Bernstein coefficients and Bernstein basis functions as follows,

$$\mathcal{D}(\tau) \approx {B_{3,t}}^{D} = \begin{bmatrix} {C_{0,t}}^{D} \\ {C_{1,t}}^{D} \\ {C_{2,t}}^{D} \\ {C_{3,t}}^{D} \end{bmatrix}^{\top} \begin{bmatrix} \beta_{0,3}(\tau) \\ \beta_{1,3}(\tau) \\ \beta_{2,3}(\tau) \\ \beta_{3,3}(\tau) \end{bmatrix} = \boldsymbol{D}_t \boldsymbol{\beta}_t \tag{9}$$

where $\boldsymbol{D}_t$ and $\boldsymbol{\beta}_t$ are vectors of Bernstein coefficients and basis functions for the tth interval respectively. Likewise, the forecasted RES can also be defined with such vectors. The subscripts of the coefficient C are its indices and its superscript is what the coefficient is describing (here the demand).

2.3.2. Bernstein zero-order continuity

The Bernstein polynomials that describe power during the time interval should be continuous, even at the joint point of the adjutant intervals. To preserve zero-order continuity between intervals, the first Bernstein coefficient of tth interval should be equal to the last Bernstein coefficient of the previous interval. Zero-order continuity prevents generation units from jumping in power.

$${C_{0,t,i}}^{p} = {C_{3,t-1,i}}^{p} \quad t \in T,\ i \in \mathcal{I} \tag{10}$$

As SU and SD trajectories are considered, Eq. (10) will be maintained when units start-up or shut down.

2.3.3. Bernstein first-order continuity

Furthermore, it is physically impossible to have instant changes in ramping. Accordingly, the differential of the Bernstein polynomials that describe power should also be continuous. According to Eq. (4), this constraint is given by,

$${C_{1,t,i}}^{p} - {C_{0,t,i}}^{p} = {C_{3,t-1,i}}^{p} - {C_{2,t-1,i}}^{p} \quad t \in T,\ i \in \mathcal{I} \tag{11}$$

Again, as SU and SD trajectories are considered, Eq. (11) will be maintained when units start-up or shut down.

2.3.4. Power balance

The sum of the generation should meet the demand over the time horizon. According to Proposition 2.3 we can sum over the coefficients of the Bernstein polynomials that represent the generation. The power balance for each hour can be written as,

$$\sum_{i\in\mathcal{I}} (\boldsymbol{P}_{t,i}) + \boldsymbol{P}_t^{\mathrm{RES}} - \boldsymbol{P}_t^{\mathrm{curt}} = \boldsymbol{D}_t \tag{12}$$

where $\boldsymbol{P}$, $\boldsymbol{P}^{\mathrm{RES}}$, and $\boldsymbol{P}^{\mathrm{curt}}$ are vectors of Bernstein coefficients for thermal generation, RES generation, and RES curtailment, respectively. The equivalent of Eq. (12) in term of the coefficients will be,

$$\sum_{i\in\mathcal{I}} ({C_{b,t,i}}^{p}) + {C_{b,t}}^{\mathrm{RES}} - {C_{b,t}}^{\mathrm{curt}} = {C_{b,t}}^{D} \quad t \in T,\ i \in \mathcal{I},\ \forall b \tag{13}$$

2.3.5. SU and SD trajectories

As mentioned before, the thermal generation also includes the SU and SD trajectories. Considering SU and SD trajectories allows having a fully continuous representation of power generation throughout the time horizon. The generation will be continuous even on start-up and shut-down of the units, so no further adjustment in the modeling is required to allow start-up and shut-down of the units. A sample sequence is illustrated in Fig. 4 to show the SU and SD trajectories for a unit with $\mathrm{SU}_i^T = \mathrm{SD}_i^T = 1$, the binary variable, and the corresponding Bernstein coefficients. In Fig. 4, for instance $C_{0,7}$ is the first Bernstein coefficient when $t = 7$. For the sake of brevity, the superscript of coefficient C describing power outputs is not shown.

2.3.6. Generation capacity

According to Eq. (5), the following inequality would be enough to preserve the capacity of units within their limits,

$$\underline{P}_i \le {C_{b,t,i}}^{p} \le \overline{P}_i \quad t \in T,\ i \in \mathcal{I},\ \forall b \tag{14}$$

where b is the index of Bernstein coefficients.

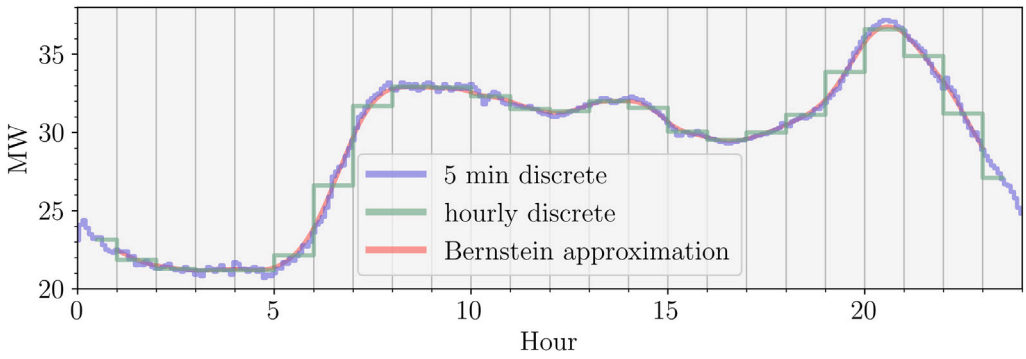

Fig. 3. Hourly discrete, 5 min discrete, and Bernstein approximation of load. The maximum deviation of hourly discrete approximation from 5 min discrete data is 3.005 MW and the mean absolute error is 0.528 MW, while the max deviation for Bernstein approximation is 0.67 MW and the mean absolute error is 0.183 MW.

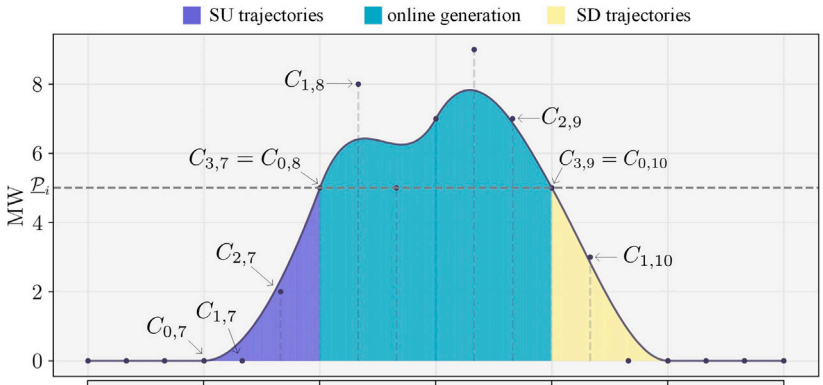

t	7	8	9	10	11
u_i	0	1	1	1	0
v_i	0	1	0	0	0
w_i	0	0	0	1	0

Fig. 4. An illustrative sequence of binary variables, SU, and SD trajectories for unit i.

2.3.7. Ramping capacity

Using Eq. (4), the following equation is concluded for the differential of a Bernstein polynomial of order three,

$$B'_{3,t,i} = 3\begin{bmatrix} {C_{1,t,i}}^p - {C_{0,t,i}}^p \\ {C_{2,t,i}}^p - {C_{1,t,i}}^p \\ {C_{3,t,i}}^p - {C_{2,t,i}}^p \end{bmatrix}^\top \begin{bmatrix} \beta_{0,2}(\tau) \\ \beta_{1,2}(\tau) \\ \beta_{2,2}(\tau) \end{bmatrix} \tag{15}$$

Which is defined by Bernstein's basis functions of order 2. By referring to Eq. (5) the ramping constraint can be written as,

$$\underline{\mathcal{R}}_i \le {C_{b,t,i}}^p - {C_{b-1,t,i}}^p \le \overline{\mathcal{R}}_i \quad t \in T,\ i \in \mathcal{I},\ b \in \{1,2,3\} \tag{16}$$

2.4. CFCUC formulation additions

2.4.1. RoCoF constraint

The RoCoF constraint is straightforward, as it is linearly derived from the well-known swing equation. Assuming that the power of the lost unit is described with a vector of Bernstein coefficients, $\boldsymbol{P}_{t,\ell}$, according to Eq. (5) the following constraint will be enough to ensure RoCoF restrictions,

$$\boldsymbol{P}_{t,\ell} \le \frac{2\Delta f'_{\text{crit}}}{f_0} \sum_{i \in \mathcal{I}, i \neq \ell} (H_i \mathcal{M}_i u_{t,i}) \ \ t \in T,\ \forall \ell \tag{17}$$

where ℓ is the index of the lost generator, $\Delta f'_{crit}$ is the critical RoCoF, H is the inertia, and $\mathcal{M}$ is the base power of the unit. Note that $\boldsymbol{P}$ contains the Bernstein coefficients.

2.4.2. Steady state frequency constraint

A linear steady-state frequency constraint can be derived from the swing equation. It is assumed that frequency is converged and there has been enough time for units to deliver their reserve power. To make sure that the steady state frequency is not violated, this constraint can be derived from the swing equation,

$$\sum_{i \in \mathcal{I}, i \neq \ell} \boldsymbol{R}_{t,i} \ge \boldsymbol{P}_{t,\ell} - D\boldsymbol{D}_i \Delta f^{\text{ss}}_{\text{crit}} \ \ t \in T,\ \forall \ell \tag{18}$$

This constraint is very similar to the reserve constraint traditionally used in the UC problem.

2.4.3. Frequency nadir constraint

Unlike the previous two constraints, the frequency nadir is more complicated to drive from the swing equation. An essential assumption to drive the frequency nadir is that the units can deliver their headroom linearly and in T^g seconds [7,8]. The continuous representation of the frequency nadir is given by,

$$f^{\text{nadir}}(\tau) = \frac{f_0 T^g p_\ell(\tau)^2}{4 r_\ell(\tau) H_\ell - D T^g f_0 D(\tau) p_\ell(\tau)} \tag{19}$$

where H_ℓ is the available weighted inertia after outage. Note that H_ℓ is only a variable of u and is constant during each hourly interval. Additional information regarding the derivation of Eq. (19) from the swing equation is elaborated upon in [32].

Assuming that all of the continuous elements in Eq. (19) are described by Bernstein polynomials of order 3 in hourly intervals, the

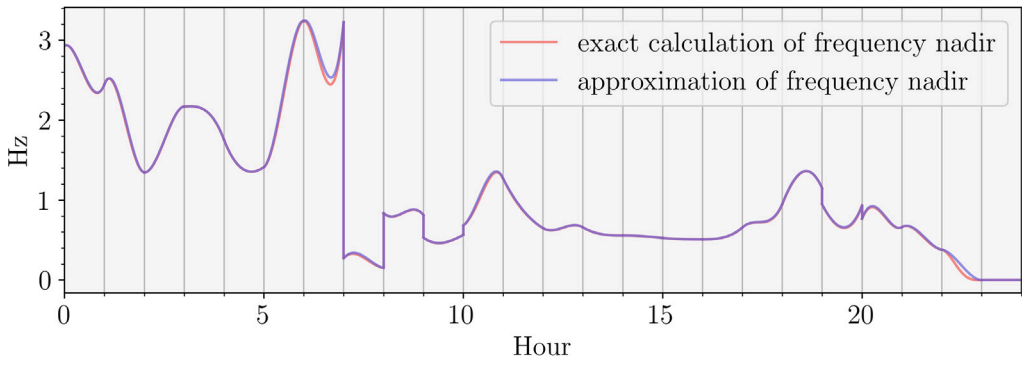

Fig. 5. The exact calculation of Eq. (19) is compared with the approximation in Eq. (21).

term in the numerator includes a square of a Bernstein polynomial of order 3, which leads to a Bernstein polynomial of order 6 (see Proposition 2.5). The first term in the denominator is a product of a Bernstein polynomial of order 3 in a constant for each interval (remember that we assumed u can only change at the beginning of the hourly intervals). The second term in the denominator includes a product of the Bernstein polynomial of order 3 into another Bernstein polynomial of order 3, which again leads to a Bernstein polynomial of order 6. To calculate the denominator, the order of the first term should be elevated based on Proposition 2.4 from 3 to 6. Then the frequency nadir will be described by a fraction, where nominator and denominator are Bernstein polynomials of order 6. The coefficients can be calculated based on the coefficients of the initial Bernstein polynomials of order 3, but that will cause a temporal dependency i.e. some of the coefficients will be dependent on the previous or the following control points. This is very hard to calculate, let alone the non-linearities, and the process of applying it to the MILP problem at hand. Let $p_\ell(\tau) = B_3{}^p$, $r_\ell(\tau) = B_3{}^r$, and $D(\tau) = B_3{}^D$ (we defined continuous variables in Eq. (19) as Bernstein polynomials of order 3). To simplify the calculation of frequency nadir we make these assumptions,

$$(B_3{}^p)^2 \approx \left[(C_0{}^p)^2 \quad (C_1{}^p)^2 \quad (C_2{}^p)^2 \quad (C_3{}^p)^2\right] \boldsymbol{\beta}_t \tag{20a}$$

$$B_3{}^D B_3{}^p \approx \left[C_0{}^D C_0{}^p \quad C_1{}^D C_1{}^p \quad C_2{}^D C_2{}^p \quad C_3{}^D C_3{}^p\right] \boldsymbol{\beta}_t \tag{20b}$$

These assumptions eliminate the temporal dependency and let us define the nominator and denominator of Eq. (19) as Bernstein polynomials of order 3, like any other continuous variable in this paper. Note that for the sake of brevity, the indices of time and units are not shown in Eqs. (20a) and (20b). The coefficients of the approximated frequency nadir will be calculated as,

$$C_{b,t,\ell}{}^f = \frac{f_0 T^g (C_{b,t,\ell}{}^p)^2}{4 C_{b,t,\ell}{}^r H_{t,\ell} - D T^g f_0 C_{b,t,\ell}{}^D C_{b,t,\ell}{}^p} \tag{21}$$

Both exact calculation and approximation of frequency nadir are shown in Fig. 5. Fig. 5 shows the frequency nadir caused by the outage of a sample unit throughout the day and confirms that the approximation in Eqs. (20a) and (20b) is reasonable.

Considering that even the approximated version of Eq. (19) is non-linear and applying it to the problem at hand would be challenging, we propose a data-driven method to drive the frequency nadir constraint. The dataset is synthetically built, using the algorithm proposed in [14]. The algorithm is also presented in Appendix. For the purpose of this paper, lost power, online inertia, and available reserve are chosen as features, as they are the variables appearing in Eq. (19). To label each sample, the frequency nadir is calculated using Eq. (21). Utilizing this labeled dataset, and with the help of a classic machine learning method (regression in this paper), a linear constraint on frequency nadir can be attained. According to Eq. (5), this constraint will prevent outages in which the frequency nadir will exceed the specified critical value.

$$\alpha_0 + \alpha_1 C_{b,t,\ell}{}^p + \alpha_2 H_\ell + \alpha_3 C_{b,t,\ell}{}^r \leq \Delta f_{\text{crit}}^{\text{nadir}} \tag{22}$$

The effectiveness, accuracy, and applicability of a data-driven constraint depend on many factors, including the quality of the dataset in reflecting the behavior of the system, the complexity of learning labels, and the cross-validation score of the learned constraint, among others. Later in the result section, the precision of Eq. (22) in learning frequency nadir is proven for the case study.

2.4.4. Summary of the proposed formulation

The proposed continuous FCUC is solved with the objective of minimizing Eq. (8a). The binary logic of the problem is similar to Eqs. (8b) to (8e) with minimal changes. The power balance equality is defined in Eq. (8j). Zero-order and first-order continuity are necessary to ensure that the scheduled power and ramp are continuous and are assured by Eqs. (10) and (11), respectively. Generation and ramping capacity limitations are forced by Eqs. (14) and (16), respectively. The frequency-related constraints considered in this paper are RoCoF, steady-state frequency, and frequency nadir constraints. RoCoF and steady-state frequency constraints are linearly derived from the swing equation and are presented in Eqs. (17) and (18). Then it is argued that the continuous frequency nadir is hard to implement in an MILP formulation analytically, so a data-driven method is introduced alternatively, leading to Eq. (22).

3. Numerical results

The proposed methodology is applied to real data of a sample day on the Spanish island of La Palma. La Palma power system comprises 11 generation units and has a peak demand of around 40 MW. As it is a system dominated by fast diesel units, T^g in Eq. (19) is assumed to be 3 s, and a load damping factor (D) of 1% is assumed. The optimization problem has been written in GAMS and solved by the Gurobi solver [33]. For the sake of comparison, three cases are defined, and the results are compared.

- **CUC**: the standard continuous UC without the frequency-related constraints similar to the one presented in [19] but with the additional SU and SD constraints.
- **RoCoF-CUC**: the proposed CFCUC minus the frequency nadir constraint.
- **CFCUC**: the complete CFCUC formulation summarized in Section 2.4.4. Different frequency nadir thresholds are showcased to better demonstrate the effectiveness of the proposed method.

All of the inputs, codes, and results of this study are available online. The interested reader is referred to [34] at https://doi.org/10.5281/zenodo.10401279.

A summary of the obtained results for the three cases is presented in Table 1. The operation cost of CUC is less than the other cases, as there are no frequency-related constraints to prevent poor frequency responses. And as expected, the operation cost gets more expensive as

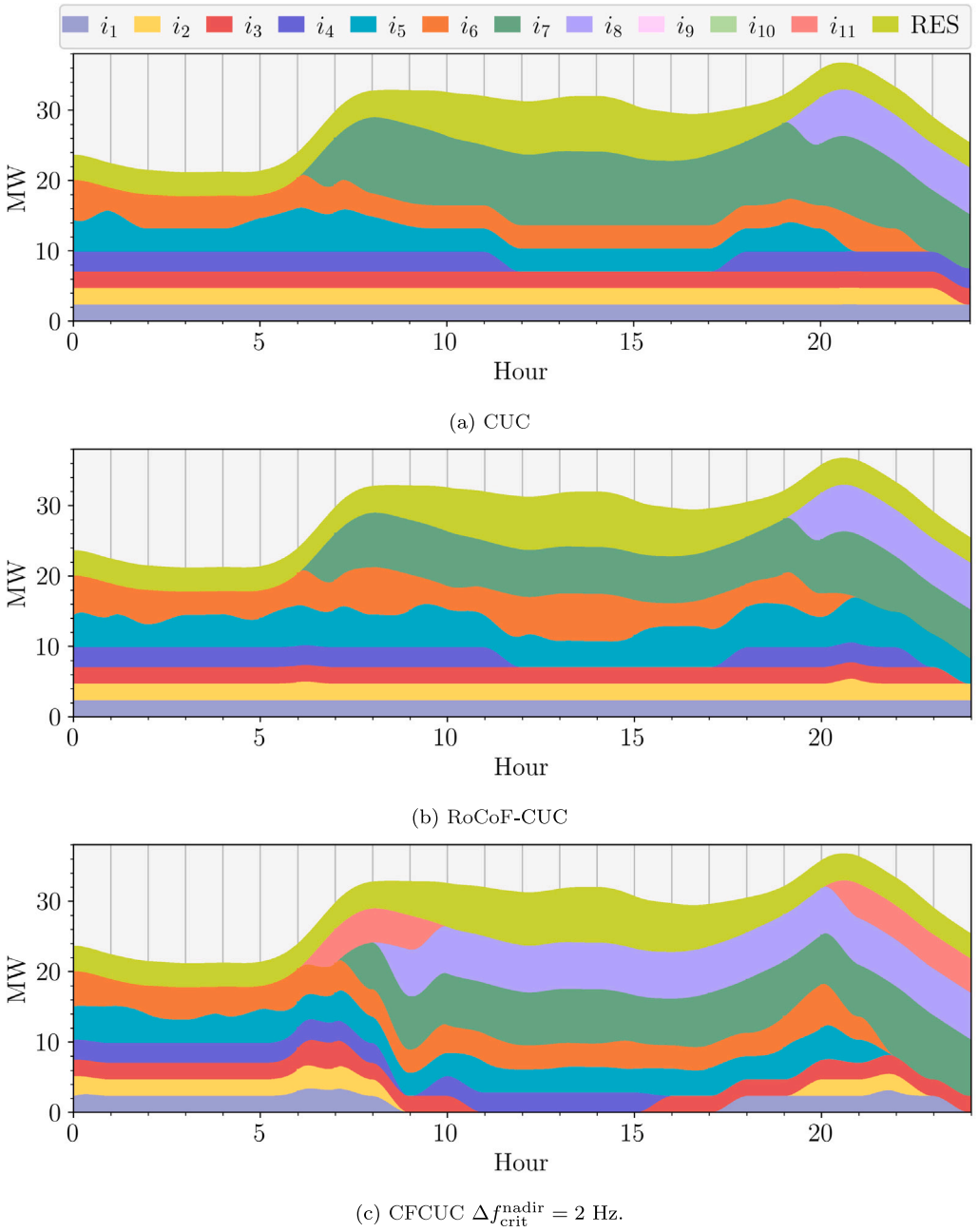

Fig. 6. Generation schedule of RES and the units i_1 to i_{11} for (a) CUC, (b) RoCoF-CUC, and (c) CFCUC when $\Delta f_{\text{crit}}^{\text{nadir}}$ is 2 Hz. Each hour is defined with a Bernstein polynomial of order 3.

Table 1
Summary of the results.

Case	$\Delta f^{\text{nadir}} > 2.5$ Hz	Operation cost	Run-time	Score
CUC	1151′	118.03 k€	82″	–
RoCoF-CUC	677′	118.54 k€	52″	–
CFCUC $\Delta f_{\text{crit}}^{\text{nadir}} = 3$ Hz	556′	118.78 k€	77″	99.93%
CFCUC $\Delta f_{\text{crit}}^{\text{nadir}} = 2.5$ Hz	0′	122.48 k€	196″	99.67%
CFCUC $\Delta f_{\text{crit}}^{\text{nadir}} = 2$ Hz	0′	128.5 k€	1725″	99.61%

the constraints get more restrictive. This is the cost that the operator pays to improve the frequency response. The cost suddenly increases when frequency threshold gets tight (in the case of $\Delta f_{\text{crit}}^{\text{nadir}} = 2$ for example). But when the threshold is reasonable (in the case of $\Delta f_{\text{crit}}^{\text{nadir}} = 3$ for example), the proposed method can improve the frequency response considerably, with a minimal increment in the operation cost.

Despite the complexities of the continuous formulation and the frequency constraints, especially the frequency nadir, the proposed CFCUC is solved in a timely manner. This is mainly because of considering the SU and SD trajectories, which simplifies many parts of the continuous formulation, and also estimating the frequency nadir threshold with the linear constraint in Eq. (22). Additionally, it is important to note that

the CFCUC method is specifically designed for island power systems, which experience significant frequency drops following outages. Given that these systems are typically small, the introduction of new variables is both feasible and justified.

The cross-validated accuracy of the learning process (logistic regression) is depicted in Table 1 within the score column. In this process, 70% of the data samples serve as the training dataset, while the remaining 30% comprise the test dataset. The score reflects the accuracy of applying the learned estimation from the training dataset to the test dataset. Notably, the score exhibits a very high value, indicating that Eq. (22) can effectively identify operation points leading to a frequency nadir deviation exceeding $\Delta f_{\text{crit}}^{\text{nadir}}$ with exceptional precision. Later, it is assured in Fig. 7 that the proposed CFCUC has been able to flawlessly prevent frequency nadir deviating from $\Delta f_{\text{crit}}^{\text{nadir}}$.

In the second column, the number of minutes that the outage of a unit would lead to $\Delta f^{\text{nadir}} > 2.5$ Hz is calculated. In the CUC generation schedule during 1151 min through the day, there is a unit online whose outage will cause a frequency deviation higher than 2.5 Hz. The number of minutes reduces as the constraints get more restrictive. And when $\Delta f_{\text{crit}}^{\text{nadir}} > 2.5$ Hz is imposed, the frequency deviation is never higher than 2.5 Hz.

The scheduled generation for CUC, RoCoF-CUC, and CFCUC are shown in Figs. 6(a) to 6(c). The generation schedule for CUC and RoCoF-CUC are very similar, but it seems when the RoCoF constraint is added, the generation of units 5 and 6 is increased to reduce the generation of unit 7, to prevent the big outages that were violating RoCoF limitation. Then for the CFCUC with a restricting $\Delta f_{\text{crit}}^{\text{nadir}}$ of 2 Hz, the combination of online units further changes to keep the frequency nadir deviation below the critical value throughout the day, by committing units with higher inertia and by preventing relative big power outages.

To better compare how the proposed CFCUC has been able to improve the frequency response by preventing poor frequency incidents from happening, the exact calculated frequency nadir from Eq. (19) for all the online units throughout the day is shown in Fig. 7. It can be seen in Figs. 7 and 7(b) to 7(d) how the frequency nadir constraint in Eq. (22) has been able to perfectly prevent frequency nadir deviation to go over $\Delta f_{\text{crit}}^{\text{nadir}}$, although the frequency nadir calculated in Eq. (19) has been approximated once with Eqs. (20a) and (20b) and then estimated with a learning process in Eq. (22). This further proves the accuracy of approximation of Eqs. (20a) and (20b) (as showed also before in Fig. 5) and the machine learning method that is used. Something else that is evident in Fig. 7 is that intra-hour changes in the frequency nadir deviation can be substantial. In some hours the deviation can differ by more than 2 Hz during the same hour. Something that has been ignored in the traditional discrete FCUC. For example in CUC at hour 8, the schedule generation of unit i_7 increases a lot, so the frequency nadir deviation at the end of the hour is around 2.5 Hz more comparing to the beginning of the hour if the unit fails. Moreover, if unit i_7 fails during the first half of hour 8, the frequency deviation remains within 3 Hz. However, if the failure occurs in the second half, the deviation exceeds 3 Hz. This clearly demonstrates the inadequacy of hourly UC in capturing these fluctuations in frequency response. Another noteworthy observation from Fig. 7 is the abrupt changes in frequency nadir between adjacent intervals, attributed to the sudden decrease or increase in online inertia due to the shutdown or startup of new units. For instance, in Fig. 7(a), the frequency nadir following the outages of i_7 and i_8 deteriorates towards the end of the day as multiple units shut down.

4. Conclusion

This paper introduces a CFCUC approach designed to mitigate the impact of intra-hour real-time power fluctuations on system frequency, thereby preventing undesirable frequency responses that could fall below critical thresholds. The presented results demonstrate the efficacy of the proposed model, showcasing its ability to be solved efficiently while achieving the intended goal of maintaining the quality of frequency response. This approach represents a significant advancement in addressing the unit commitment problem within a continuous-time framework, offering improved accuracy and computational efficiency in handling frequency-related constraints. The utilization of a data-driven frequency nadir constraint method in this study proves effective, affirming the reasonability of the simplifying assumptions adopted. As the proposed data-driven frequency nadir constraint is effective, while not imposing much computational burden on the UC problem, its usage is recommended, as a substitute for analytical methods that require extensive linearization.

This research contributes valuable insights into ensuring reliable and stable power system operations against dynamic real-time changes. The next step for this line of research can be applying the method to bigger inertia systems, and also considering under-frequency load-shedding, which is much more challenging to implement in an MILP formulation. Another direction is to approximate the frequency response curve with the Bernstein Polynomials and implement in the CUC.

CRediT authorship contribution statement

Mohammad Rajabdorri: Writing – original draft, Visualization, Methodology, Investigation, Conceptualization, Data curation, Formal analysis, Resources, Software, Validation. **Enrique Lobato:** Writing – review & editing, Supervision, Formal analysis, Funding acquisition, Resources, Validation. **Lukas Sigrist:** Writing – review & editing, Supervision, Formal analysis, Funding acquisition, Resources, Validation. **Jamshid Aghaei:** Formal analysis, Validation, Writing – review & editing.

Declaration of competing interest

There is no conflict of interest.

Acknowledgments

This research has been funded by grant PID2022-141765OB-I00 funded by MCIN/AEI/10.13039/501100011033 and by “ERDF A way of making Europe”

Appendix

The synthetic data generation algorithm is from [14] and is provided here,

In summary, algorithm 1 enumerates all possible combinations of power generation in a discrete manner. However, many of these combinations may not be feasible, as they might not satisfy the UC constraints such as power balance, reserve requirements, or minimum RoCoF. We retain only the combinations that meet these UC constraints. Our focus is on the combinations that the optimization problem might select as the optimal solution. Therefore, we sort the feasible combinations and eliminate the more expensive ones, as they are less likely to be chosen as the UC solution.

Data availability

All the data and results are uploaded and included.

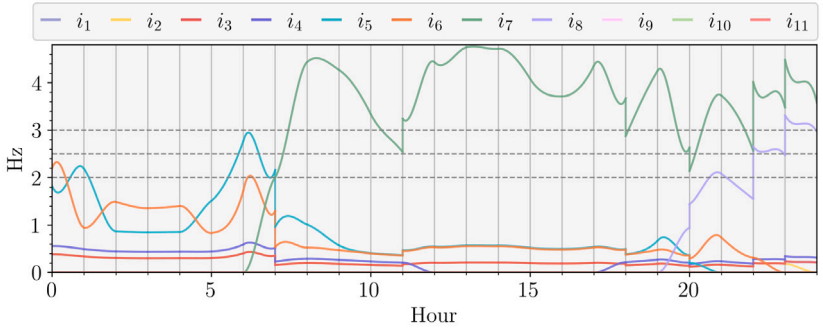

(a) CUC

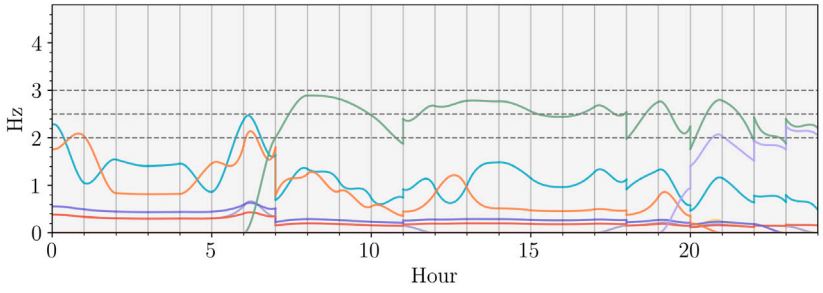

(b) CFCUC $\Delta f_{\text{crit}}^{\text{nadir}} = 3$ Hz

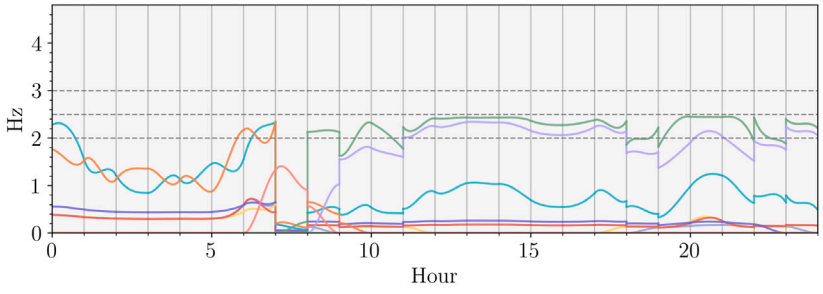

(c) CFCUC $\Delta f_{\text{crit}}^{\text{nadir}} = 2.5$ Hz

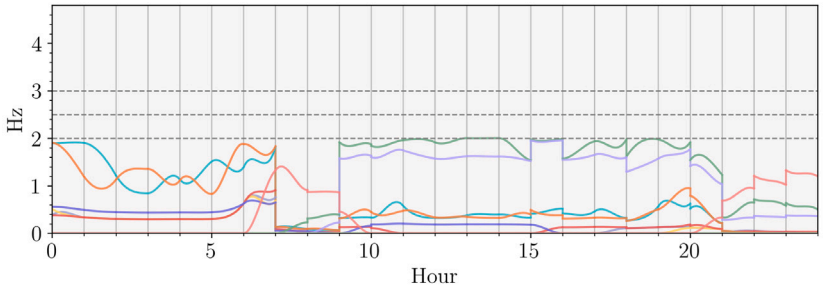

(d) CFCUC $\Delta f_{\text{crit}}^{\text{nadir}} = 2$ Hz

Fig. 7. Frequency nadir calculated by Eq. (19) of the units i_1 to i_{11} committed by (a) CUC, (b) CFCUC with $\Delta f_{\text{crit}}^{\text{nadir}} = 3$ Hz, (c) CFCUC with $\Delta f_{\text{crit}}^{\text{nadir}} = 2.5$ Hz, (d) CFCUC with $\Delta f_{\text{crit}}^{\text{nadir}} = 2$ Hz.

Algorithm 1 Synthetic Data Generation

Inputs: $\overline{D}$, $\underline{D}$, $\overline{P}_i$, Δf, f_0, H_i, M_i
Output: $\mathcal{F}$: set of feasible power level vectors

$\mathcal{F} \leftarrow \emptyset$
for $\vec{p} \in \bigtimes_{i=1}^{I} \mathcal{P}_i$ **do** ▷ for all power level vectors
  for $i \in \{1, \dots, I\}$ **do** ▷ for every generator
    $u_i := 0$ if $p_i = 0$ else 1 ▷ status of unit
  end for
  $G := \sum_{i=1}^{I} p_i$ ▷ total generation
  $R_\ell := \left(\sum_{i=1}^{I} u_i(\overline{P}_i - p_i) \right) - u_\ell(\overline{P}_\ell - p_\ell)$ ▷ reserve after outage of ℓ
  $H_\ell^{\text{sys}} := (\sum_{i=1}^{I} H_i M_i u_i) - H_\ell M_\ell u_\ell$ ▷ inertia after outage of ℓ
  if $\underline{D} \le G \le \overline{D}$ and $R_\ell \ge p_\ell$ and $H_\ell^{\text{sys}} \ge \frac{p_\ell f_0}{2\Delta f}$ **then** ▷ feasible?
    $\mathcal{F} \leftarrow \mathcal{F} \cup \{\vec{p}\}$ ▷ add power level vector
  end if
end for
Sort $\mathcal{F}$ ascending by the quadratic generation cost function
Keep a reasonable number of cheaper combinations and remove the rest

$\overline{D}$ and $\underline{D}$ are lower and upper bounds on yearly thermal generation (MW), i is the index of unit $\in \{1, \dots, I\}$, $\overline{P}_i$ is the capacity of unit i (MW), Δf is critical RoCoF (Hz/s), f_0 is nominal frequency (Hz), $\mathcal{P}_i$ is the finite set of power levels of unit i including level 0 for not committed (MW), ℓ is the index of the lost unit (can be any i), H_i is the inertia of unit i, and M_i is the base power of unit i.

References

[1] Lin W, Wu D, Boulet B. Spatial-temporal residential short-term load forecasting via graph neural networks. IEEE Trans Smart Grid 2021;12(6):5373–84.
[2] Jiao R, Wang S, Zhang T, Lu H, He H, Gupta BB. Adaptive feature selection and construction for day-ahead load forecasting use deep learning method. IEEE Trans Netw Serv Manag 2021;18(4):4019–29.
[3] Duan J, Wang P, Ma W, Fang S, Hou Z. A novel hybrid model based on nonlinear weighted combination for short-term wind power forecasting. Int J Electr Power Energy Syst 2022;134:107452.
[4] Li D, Sun G, Miao S, Gu Y, Zhang Y, He S. A short-term electric load forecast method based on improved sequence-to-sequence GRU with adaptive temporal dependence. Int J Electr Power Energy Syst 2022;137:107627.
[5] CAISO S. Business practice manual for market operations. 2022, URL https://bpmcm.caiso.com/.
[6] Zhang G, Ren J, Zeng Y, Liu F, Wang S, Jia H. Security assessment method for inertia and frequency stability of high proportional renewable energy system. Int J Electr Power Energy Syst 2023;153:109309.
[7] Badesa L, Teng F, Strbac G. Simultaneous scheduling of multiple frequency services in stochastic unit commitment. IEEE Trans Power Syst 2019;34(5):3858–68.
[8] Trovato V, Bialecki A, Dallagi A. Unit commitment with inertia-dependent and multispeed allocation of frequency response services. IEEE Trans Power Syst 2018;34(2):1537–48.
[9] Zhou B, Jiang R, Shen S. Frequency stability-constrained unit commitment: Tight approximation using Bernstein polynomialss. IEEE Trans Power Syst 2023.
[10] Lagos D, Hatziargyriou ND. Data-driven frequency dynamic unit commitment for island systems with high RES penetration. IEEE Trans Power Syst 2021.
[11] Zhang Y, Chen C, Liu G, Hong T, Qiu F. Approximating trajectory constraints with machine learning–microgrid islanding with frequency constraints. IEEE Trans Power Syst 2020;36(2):1239–49.
[12] Sang L, Xu Y, Yi Z, Yang L, Long H, Sun H. Conservative sparse neural network embedded frequency-constrained unit commitment with distributed energy resources. IEEE Trans Sustain Energy 2023.
[13] Rajabdorri M, Lobato E, Sigrist L. Robust frequency constrained uc using data driven logistic regression for island power systems. IET Gen Transm Distrib 2022;16(24):5069–83.
[14] Rajabdorri M, Kazemtabrizi B, Troffaes M, Sigrist L, Lobato E. Inclusion of frequency nadir constraint in the unit commitment problem of small power systems using machine learning. Sustain Energy Grids Netw 2023;36:101161.
[15] Stankovski A, Gjorgiev B, Locher L, Sansavini G. Power blackouts in europe: Analyses, key insights, and recommendations from empirical evidence. Joule 2023;7(11):2468–84.
[16] Jiang S, Wu C, Gao S, Pan G, Wang S, Liu Y, Zhao X. Coordinative frequency-constrained unit commitment model for hvdc interconnected AC systems. Int J Electr Power Energy Syst 2022;141:108176.
[17] Han R, Hu Q, Zhang H, Ge Y, Quan X, Wu Z. Robust allocation of distributed energy storage systems considering locational frequency security. Int J Electr Power Energy Syst 2024;157:109903.
[18] Li Z, Xie X, Cheng Z, Zhi C, Si J. A novel two-stage energy management of hybrid AC/DC microgrid considering frequency security constraints. Int J Electr Power Energy Syst 2023;146:108768.
[19] Parvania M, Scaglione A. Unit commitment with continuous-time generation and ramping trajectory models. IEEE Trans Power Syst 2015;31(4):3169–78.
[20] Scaglione A. Continuous-time marginal pricing of power trajectories in power systems. In: 2016 information theory and applications workshop. ITA, IEEE; 2016, p. 1–6.
[21] Bagherinezhad A, Khatami R, Parvania M. Continuous-time look-ahead flexible ramp scheduling in real-time operation. Int J Electr Power Energy Syst 2020;119:105895.
[22] Zhou B, Ai X, Fang J, Li K, Yao W, Chen Z, Wen J. Function-space optimization to coordinate multi-energy storage across the integrated electricity and natural gas system. Int J Electr Power Energy Syst 2023;151:109181.
[23] Morales-España G, Ramos A, García-González J. An MIP formulation for joint market-clearing of energy and reserves based on ramp scheduling. IEEE Trans Power Syst 2013;29(1):476–88.
[24] Morales-España G, Latorre JM, Ramos A. Tight and compact MILP formulation of start-up and shut-down ramping in unit commitment. IEEE Trans Power Syst 2012;28(2):1288–96.
[25] Gentile C, Morales-Espana G, Ramos A. A tight MIP formulation of the unit commitment problem with start-up and shut-down constraints. EURO J Comput Optim 2017;5(1–2):177–201.
[26] Morales-España G, Ramírez-Elizondo L, Hobbs BF. Hidden power system inflexibilities imposed by traditional unit commitment formulations. Appl Energy 2017;191:223–38.
[27] Shi Y, Li Y, Zhou Y, Xu R, Feng D, Yan Z, Fang C. Optimal scheduling for power system peak load regulation considering short-time startup and shutdown operations of thermal power unit. Int J Electr Power Energy Syst 2021;131:107012.
[28] Lorentz GG. Bernstein polynomials. American Mathematical Soc.; 2012, p. 3–5.
[29] Dierckx P. Curve and surface fitting with splines. Oxford University Press; 1995.
[30] Parvania M, Scaglione A. Generation ramping valuation in day-ahead electricity markets. In: 2016 49th Hawaii international conference on system sciences. HICSS, IEEE; 2016, p. 2335–44.
[31] Kielas-Jensen C, Cichella V, Berry T, Kaminer I, Walton C, Pascoal A. Bernstein polynomial-based method for solving optimal trajectory generation problems. Sensors 2022;22(5):1869.
[32] Ferrandon-Cervantes C, Kazemtabrizi B, Troffaes MC. Inclusion of frequency stability constraints in unit commitment using separable programming. Electr Power Syst Res 2022;203:107669.
[33] Gurobi Optimization L. Gurobi Optimizer Reference Manual. 2023, URL https://www.gurobi.com.
[34] Rajabdorri M. Data-Driven Continuous-Time Framework for Frequency-Constrained Unit Commitment. 2023, http://dx.doi.org/10.5281/zenodo.10401279.